Article

D$_1$-A-D$_2$ Conjugated Porous Polymers Provide Additional Electron Transfer Pathways for Efficient Photocatalytic Hydrogen Production

Zheng-Hui Xie [1,†], Yu-Jie Zhang [1,†], Jinhua Li [1,*] and Shi-Yong Liu [1,2,*]

[1] Jiangxi Provincial Key Laboratory of Functional Crystalline Materials Chemistry, School of Chemistry and Chemical Engineering, Jiangxi University of Science and Technology, Ganzhou 341000, China; stillonge@outlook.com (Z.-H.X.); 15079698527@163.com (Y.-J.Z.)

[2] School of Chemical Engineering, Guangdong University of Petrochemical Technology, Maoming 525000, China

[*] Correspondence: lijh@jxust.edu.cn (J.L.); chelsy@jxust.edu.cn or chelsy@zju.edu.cn (S.-Y.L.)

[†] These authors contributed equally to this work.

Abstract: The strategic design of donor–acceptor (D-A) conjugated porous polymers has emerged as a pivotal methodology for advancing efficient photocatalytic hydrogen evolution. However, conventional D-A polymeric architectures face inherent limitations: excessively strong acceptor units may lower the LUMO energy level, compromising proton (H$^+$) reduction capability, while weak D-A interactions result in inadequate light-harvesting capacity and insufficient photogenerated electrons, ultimately diminishing photocatalytic activity. To address these challenges, we developed a new D1-A-D2 conjugated porous polymer (CPP) system. The strategic incorporation of a secondary donor benzothiophene (DBBTh) unit enabled precise bandgap engineering in D$_1$-A-D$_2$ CPPs. Experimental results demonstrate that DBBTh integration significantly enhances both light absorption efficiency and proton reduction ability. Under visible-light irradiation (λ > 420 nm), the Py-BKh1 photocatalyst achieved a hydrogen evolution rate (HER) of 10.2 mmol h^{-1} g^{-1} with an apparent quantum yield (AQY) of 9.5% at 500 nm. This work provides a groundbreaking paradigm for designing high-performance organic photocatalysts.

Keywords: π-conjugated porous polymers; direct C–H arylation polymerization; photocatalysis; D1-A-D2 conjugated polymer; visible-light-driven hydrogen evolution

1. Introduction

Since Fujishima's group [1] reported TiO$_2$ for water splitting under ultraviolet (UV) light (λ > 290 nm) in 1972, an increasing number of researchers have focused on photocatalytic water splitting, leading to the discovery of numerous photocatalysts. However, most of these are inorganic materials, while organic photocatalysts remain rarely reported [2–5]. A paradigm shift emerged in 1985, Yanagida's group [6] reported the use of poly(p-phenylene) (PPP) for UV-driven photocatalytic hydrogen evolution, marking the first demonstration of conjugated porous polymers as photocatalysts and revealing the potential of organic semiconductors in hydrogen production. Subsequently, in 2006, Wang's group [7] reported graphitic carbon nitride (g-C$_3$N$_4$) for solar-driven hydrogen evolution, significantly advancing global research on organic semiconductor-based photocatalytic hydrogen generation. Finally, Shi's group [8] reported the donor–acceptor (D-A) molecular design strategy—prevalent in organic solar cells—into photocatalysis, achieving

groundbreaking progress. Building on decades of research, a wide range of D-A conjugated polymer photocatalysts has now been reported [9–12].

D-A conjugated polymers (CPs) are a class of macromolecular materials composed of π-conjugated chains formed by alternating donor (D) and acceptor (A) units. These CPs are assembled from organic monomers of non-metallic elements, and the structural diversity of available monomers enables the preparation of D-A CPs with tailored configurations. Notably, the D-A molecular architecture plays a decisive role in tuning their physicochemical properties [13,14]. This stems from the strong electron push–pull interaction between D and A units, where extended π-conjugation narrows the bandgap, enhancing light-harvesting capability and solar energy utilization [15]. Additionally, this electronic interaction promotes efficient exciton dissociation into free charge carriers, which migrate along predefined pathways to the acceptor. For instance, our group [16] reported enhanced photocatalytic activity through $BTSO_2$-EDOT-based D-A CPs. The strong D-A effect amplified the optoelectronic response and accelerated exciton dissociation into mobile electrons, effectively suppressing electron–hole recombination. Under visible light, this system achieved a hydrogen evolution rate (HER) of 0.95 mmol h^{-1}/6 mg with an apparent quantum yield (AQY) of 13.6% at 550 nm. The structural tunability of CPs allows surface modification via functional group incorporation. For instance, introducing alkoxy chains significantly improves hydrophilicity, enhancing interfacial reactions and photocatalytic efficiency [17]. For example, Zwijnenburg's group [18] reported that grafting TEG (triethylene glycol) side chains onto CPs markedly increased hydrophilicity and swelling capacity, promoting water adsorption and accelerating surface reactions. This modification achieved a HER of 72.5 mmol h^{-1} g^{-1} under visible light. However, studies have indicated that the introduction of additional alkoxy chains may lead to the disruption of system planarity or reduction in chromophore density [19].

Despite the capability of D-A structured CPs to facilitate rapid exciton dissociation and enhance charge carrier separation, their molecular design presents significant challenges. Photocatalysts must satisfy the thermodynamic requirement where the lowest unoccupied molecular orbital (LUMO) energy level of the material lies more negative than the reduction potential of H_2O/H_2. Excessively strong acceptor units in D-A polymers may excessively lower the LUMO energy, rendering the CPs thermodynamically insufficient to drive hydrogen evolution. Conversely, weak D-A interactions compromise light-harvesting efficiency, limiting photogenerated electron density and diminishing photocatalytic activity. Consequently, the rational engineering of CPs with optimized bandgap widths and precisely aligned LUMO and highest occupied molecular orbital (HOMO) energy levels constitutes a critical step toward enhanced photocatalytic activity [20–29].

Introduction: A third component to regulate the monomer feeding ratio for achieving continuous and precise modulation of the bandgap has emerged as an important strategy to enhance the photocatalytic activity of D-A polymers [30–40]. For instance, Cooper's group [41] reported a series of conjugated microporous polymers (CMPs) with tunable optical bandgaps (1.94–2.95 eV) by adjusting the feeding ratio of pyrene (Py) and benzene (Ph) monomers. Systematic investigation revealed the impact of monomer composition on the light absorption range and photocatalytic hydrogen production performance. Notably, CP-CMP10 (Py:Ph = 1:1) achieved a HER of 174 μmol h^{-1} g^{-1} under visible light (λ > 420 nm) irradiation without requiring metal co-catalysts. This work marked the first demonstration of continuous modulation of the optical bandgap in organic polymers, breaking the traditional limitations of fixed bandgaps in inorganic materials. Inspired by natural systems, Jin's group [42] reported covalent triazine frameworks (CTFs) by incorporating carbazole as the donor unit, triazine as the primary acceptor (A_1), and benzothiadiazole as a secondary acceptor (A_2) to construct D-A_1-A_2 CTFs. Under visible light irradiation, the optimized

polymer exhibited an AQY of 22.8% at 420 nm and a HER of 19.3 mmol h^{-1} g^{-1}, with Pt as co-catalyst. This design highlights the synergistic advantages of multi-component systems in advancing photocatalytic efficiency.

Inspired by the aforementioned studies, we herein strategically constructed a series of ternary conjugated porous polymers (CPPs) with D-A configuration or D_1-A-D_2 configurations—denoted as Py-BKh0, Py-BKh1, Py-BKh2, and Py-BKh3—through atom economical C–H/C–Br cross-coupling reactions. These polymers were synthesized, using 1,3,6,8-tetrabromopyrene (TBPy) as the primary donor (D_1), bis(2-thienyl)ketone (BTK) as the acceptor (A), and 5,5′-dibromo-2,2′-bithiophene (DBBTh) as the secondary donor (D_2), by precisely modulating the feeding ratio between the primary and secondary donors. Experimental results demonstrate that the incorporation of the secondary donor significantly enhances the light responsiveness and reducing capacity of the CPPs. The secondary donor DBBTh facilitates the formation of additional electron transport pathways, promoting photogenerated charge separation and thereby improving photocatalytic activity. Under visible light irradiation ($\lambda \geq 420$ nm), the optimized CPPs achieved a HER of 10.2 mmol h^{-1} g^{-1} and an AQY of 9.5% at 500 nm. Our work provides novel insights into the molecular-level design of advanced D-A-type organic photocatalysts, offering a fresh perspective for developing high-efficiency photocatalytic systems.

2. Results and Discussion

2.1. Synthesis and Structural Characterization

We synthesized the D-A-type binary conjugated polymer Py-BKh0 via a green, atom-economical C–H/C–Br cross-coupling reaction [16,35–37,43–45], utilizing 1,3,6,8-tetrabromopyrene (TBPy) with a rigid planar framework and bis(2-thienyl)ketone (BTK) featuring a strong electron-withdrawing carbonyl group. Subsequently, 5,5′-dibromo-2,2′-bithiophene (DBBTh) was introduced as a secondary donor (D_2) to construct the ternary conjugated porous polymers (CPPs) with a D_1-A-D_2 configuration. Here, BTK serves as the electron acceptor (A), while TBPy and DBBTh act as electron donors (D). By strategically adjusting the relative content of the secondary donor (DBBTh) and primary donor (TBPy), three conjugated porous polymer samples—Py-BKh1, Py-BKh2, and Py-BKh3—were synthesized. The specific reaction pathway is illustrated in Figure 1a. The chemical structures of the synthesized polymers were characterized using Fourier-transform infrared (FT-IR) spectroscopy. As shown in Figures 1b and S1, the polymers share similar spectral features due to their identical building blocks. A broad vibration peak at 1600 cm^{-1} is attributed to the C=O stretching vibration, while absorption signals at 1400 cm^{-1} and 1515 cm^{-1} correspond to aromatic ring skeletal stretching vibrations. The broad peak at 820 cm^{-1} arises from the C–S–C characteristic vibration in the thiophene groups. Figures 1c and S2 show the solid-state ^{13}C NMR spectra of the polymers, with carbon atoms labeled as "*a-i*". All polymers exhibit a signal at ~177 ppm corresponding to the carbonyl group (carbon g) in BTK, while the signal at ~128 ppm belongs to the carbon atoms (a, b, c and d) in the BTPy unit. The tertiary carbon signals at the α-position of thiophene in BTK appear at ~150 ppm (carbons e and f), and the signal at ~142 ppm is attributed to the tertiary carbons at the α-position of DBBTh (carbons h and i). Notably, the DBBTh-associated signals are absent in Py-BKh0 but emerge in Py-BKh1, Py-BKh2, and Py-BKh3 with progressively increasing intensity, confirming the successful incorporation of DBBTh. The above analysis demonstrates that the trends in FTIR and ^{13}C NMR spectra are consistent, indicating the successful synthesis of target CPPs with varied DBBTh content.
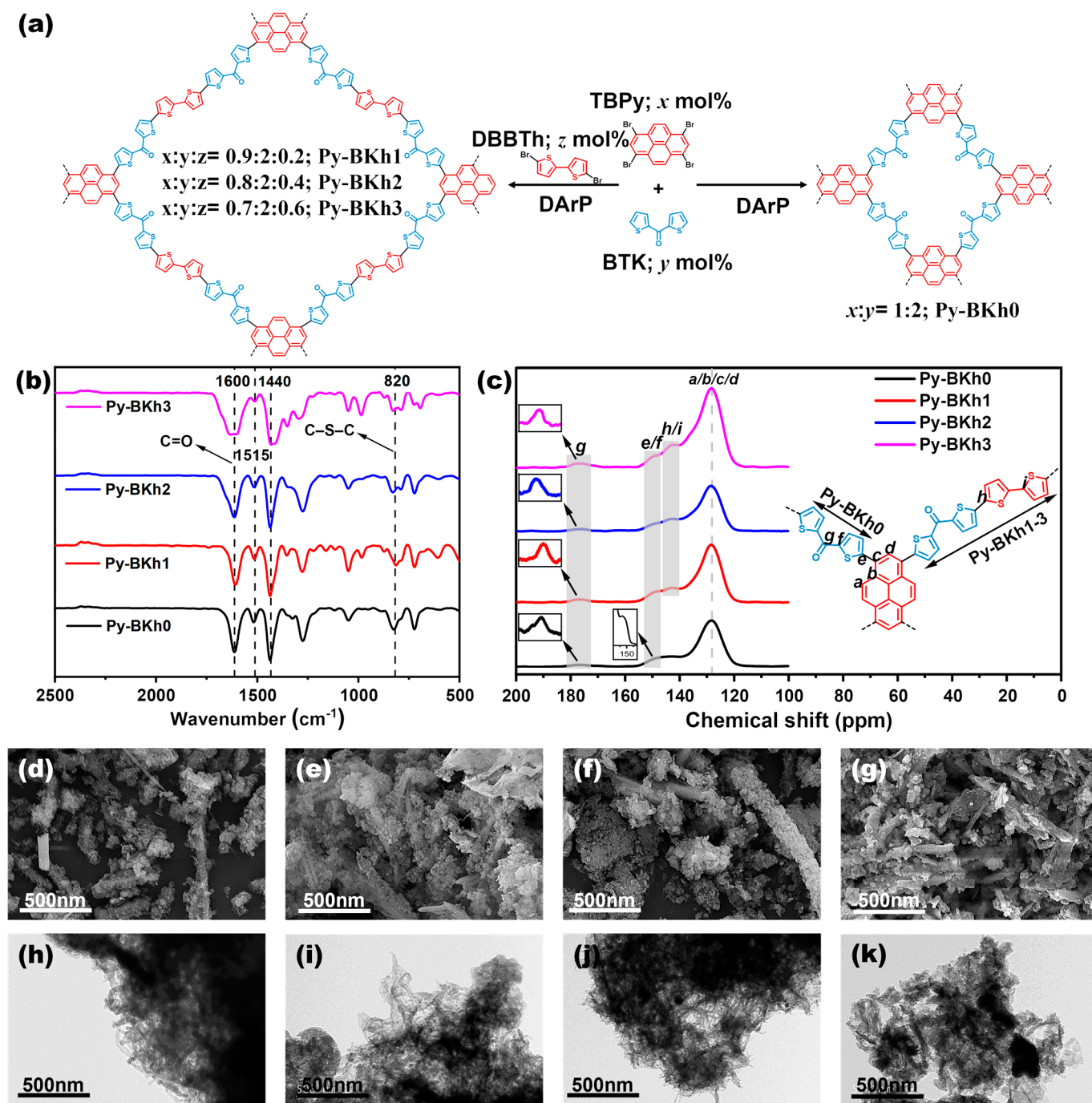
Figure 1. (**a**) Synthetic routes of Py-BKh0, Py-BKh1, Py-BKh2, and Py-BKh3; (**b**) FTIR spectra and (**c**) solid-state ^{13}C NMR spectra of all polymers; SEM images of Py-BKh0 (**d**), Py-BKh1 (**e**), Py-BKh2 (**f**), and Py-BKh3 (**g**); and TEM images of Py-BKh0 (**h**), Py-BKh1 (**i**), Py-BKh2 (**j**), and (**k**) Py-BKh3.

To investigate the effect of DBBTh content on the polymers' micromorphology, scanning electron microscopy (SEM) and transmission electron microscopy (TEM) were employed. As shown in Figure 1c–j, SEM images reveal that Py-BKh0 exhibits a mixed structure of micron-scale rods and particles with irregular dispersion, whereas Py-BKh1, Py-BKh2, and Py-BKh3 display denser layered structures. This indicates that the introduction of DBBTh modifies the surface morphology of Py-BKh0, and the layered structure facilitates the exposure of more active sites. TEM images show irregular aggregates of similar size across all samples. Figure 1g–i exhibit fibrous aggregation, while Figure 1j shows a bulk-like aggregation, suggesting that low DBBTh content has a minimal impact on

the aggregation state of Py-BKh0, but higher levels induce morphological changes. These results demonstrate that the adjustment of a secondary donor (DBBTh) content effectively modulates the micromorphology of the polymers.

2.2. Optical and Electrochemical Properties

To investigate the structure–property relationships of the polymers, we first performed ultraviolet–visible diffuse reflectance spectroscopy (UV-Vis DRS) on the four conjugated polymeric samples (Py-BKh0, Py-BKh1, Py-BKh2, and Py-BKh3). As shown in Figure 2a, all polymers exhibit strong absorption in the 300–600 nm range, with absorption edges approaching 700 nm, which facilitates visible light harvesting for photocatalytic reactions. Notably, the ternary Py-BKh1, Py-BKh2, and Py-BKh3 exhibit more redshift phenomena than that of binary Py-BKh0, with Py-BKh1 demonstrating the most bathochromic shift. This indicates that the introduction of the secondary donor DBBTh into Py-BKh0 positively enhances light absorption, and the D_1-A-D_2 ternary polymer configuration improves photon utilization. Although increasing the DBBTh content beyond optimal levels reduces light absorption, the precise control of DBBTh incorporation achieves broad absorption spectra. The optical bandgaps of the polymers, determined via the Kubelka–Munk equation using $(\alpha h v)^2$ vs. $h v$ plots (Figure 2b), are calculated as 2.08, 1.98, 2.00, and 2.02 eV for Py-BKh0, Py-BKh1, Py-BKh2, and Py-BKh3, respectively. The observed bandgap narrowing followed by widening aligns with the absorption profiles, confirming that adjustment of the TBPy: DBBTh ratio enables tuning light absorption ranges and bandgaps. Cyclic voltammetry (CV) was employed to determine the lowest unoccupied molecular orbital (LUMO) energy levels (Figure S3). After conversion to the standard hydrogen electrode, the LUMO levels are measured at −0.71, −1.02, −1.05, and −1.07 eV for Py-BKh0, Py-BKh1, Py-BKh2, and Py-BKh3, respectively. Using the relationship $E_{HOMO} = E_{LUMO} + E_g$, the highest occupied molecular orbital (HOMO) levels are calculated as 1.37, 0.96, 0.95, and 0.95 eV, respectively. The derived band structures are illustrated in Figure 2c. All polymers exhibit LUMO levels thermodynamically capable of driving hydrogen evolution. Notably, the LUMO levels of Py-BKh1, Py-BKh2, and Py-BKh3 are elevated compared to Py-BKh0, indicating enhanced driving forces for hydrogen production in the ternary polymers. Combining UV–Vis DRS, Kubelka–Munk analysis, and CV data, we demonstrate that the introduction of the secondary donor DBBTh narrows the optical bandgap to enhance light absorption, simultaneously elevating LUMO levels to strengthen photocatalytic reduction capability. These synergistic effects would have a significant impact on improving hydrogen evolution performance, highlighting the potential of molecular engineering for optimizing polymer-based photocatalysts.

The separation and transfer of photogenerated electron–hole pairs (e^--h^+) are key processes in photocatalysis. To further investigate the charge carrier separation efficiency of the polymers, we characterized the photophysical properties of the four conjugated organic polymer samples using steady-state photoluminescence (PL) spectroscopy, transient photocurrent response (TPR), and electrochemical impedance spectroscopy (EIS), as shown in Figure 2d–f. Steady-state PL spectroscopy is widely used to evaluate the radiative recombination of photogenerated charge carriers [46–49]. A higher PL intensity typically indicates stronger radiative recombination and lower charge separation efficiency, which is detrimental to photocatalytic activity. Figure 2d displays the PL intensities with a sequence of Py-BKh0 > Py-BKh3 > Py-BKh2 > Py-BKh1 under 400 nm excitation. The strong PL signal of Py-BKh0 suggests severe electron–hole recombination and poor charge separation efficiency, limiting its photocatalytic activity. In contrast, the introduction of the secondary donor DBBTh significantly suppresses PL intensity, with Py-BKh1 showing the weakest emission. This confirms that the D_1-A-D_2 ternary polymeric architecture effectively reduces

radiative recombination and enhances charge separation, thereby improving photocatalytic efficiency. TPR and EIS measurements were further conducted to evaluate charge separation dynamics. TPR analysis (Figure 2e) reveals that the ternary polymers (Py-BKh1–3) showed more enhanced photocurrent responses than that of Py-BKh0 under full-spectrum xenon lamp irradiation, indicating superior charge separation and transport capabilities in the DBBTh-modified polymers. EIS Nyquist plots (Figure 2f) demonstrate reduced charge transfer resistance for the ternary polymers, as evidenced by smaller semicircle radii. Py-BKh1 shows the smallest radius, corresponding to the lowest interfacial resistance and most efficient suppression of electron–hole recombination. These results align with the TPR results, confirming that the secondary donor DBBTh facilitates charge separation. Collectively, these characterizations demonstrate that the D_1-A-D_2 configuration promotes directional electron transfer toward acceptor units, enabling the efficient reduction of H^+ to H_2. This structural design synergistically enhances light absorption, charge separation, and catalytic activity, providing a robust strategy for developing high-performance polymeric photocatalysts.
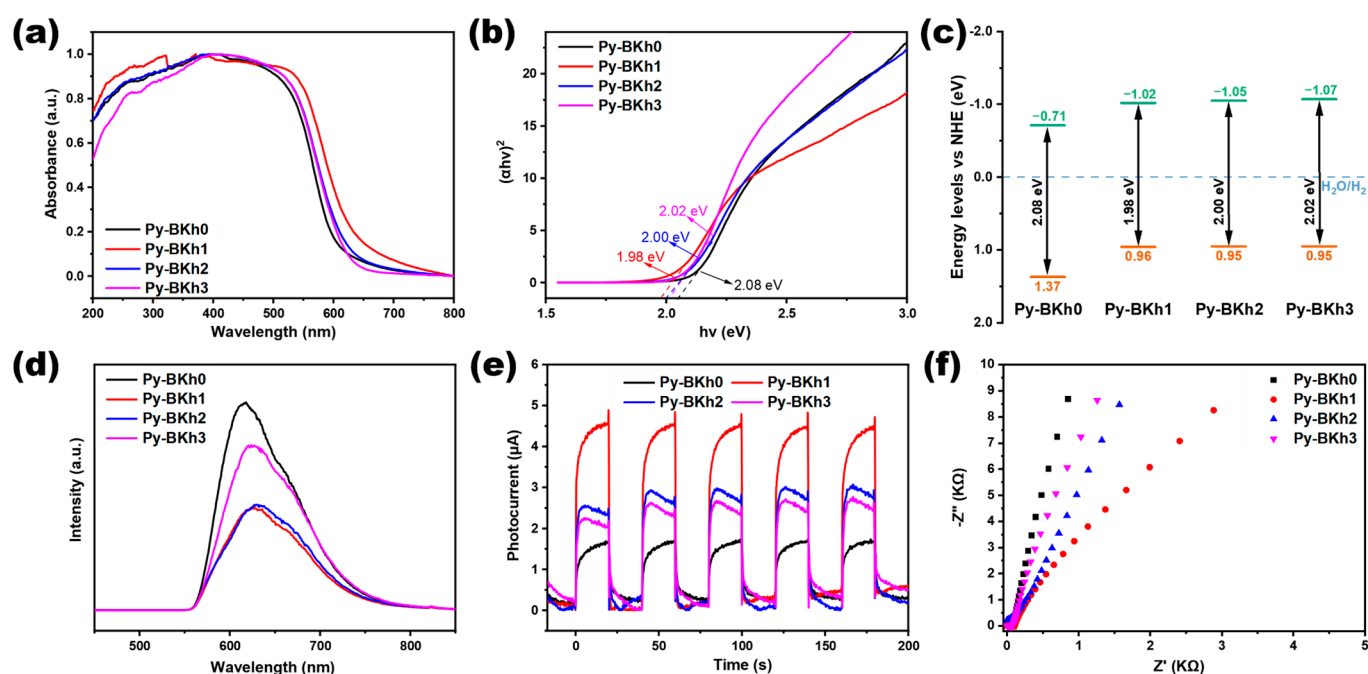

Figure 2. (**a**) UV–vis DRS. (**b**) Tauc-plot maps. (**c**) Energy band alignments. (**d**) Steady-state PL spectra. (**e**) TPR under visible light irradiation. (**f**) EIS of all CPPs.

2.3. Photocatalytic Hydrogen Production Performance

To examine the structure–performance correlations of the polymers, photocatalytic hydrogen evolution tests were conducted on Py-BKh0, Py-BKh1, Py-BKh2, and Py-BKh3 without co-catalysts. Under the condition of visible light ($\lambda \geq 420$ nm) irradiation, 6 mg polymeric catalysts, 1 M ascorbic acid as a sacrificial agent, and an NMP/H_2O (*v:v* = 1:5) mixed solvent, the hydrogen evolution rates (HERs) of Py-BKh0, Py-BKh1, Py-BKh2, and Py-BKh3 were 2.7, 61.5, 46.5, and 21.3 μmol h^{-1}, respectively (Figure 3a–b), corresponding to normalized HERs of 0.4, 10.2, 7.7, and 3.5 mmol h^{-1} g^{-1}, and no hydrogen production was observed in the absence of photocatalyst and light. Although the HER initially increased and then decreased with higher DBBTh content, all ternary systems (Py-BKh1–3) outperformed the binary counterpart (Py-BKh0), achieving 25-, 19-, and 8-fold enhancements, respectively. This demonstrates that the secondary donor DBBTh enhances light harvesting and creates energy-level gradients to suppress charge recombination,

thereby promoting charge separation and migration. Py-BKh1 exhibited the highest HER of 10.2 mmol h^{-1} g^{-1}, highlighting the critical role of optimizing the TBPy:DBBTh ratio in tuning energy-level structures for improved photocatalytic activity.
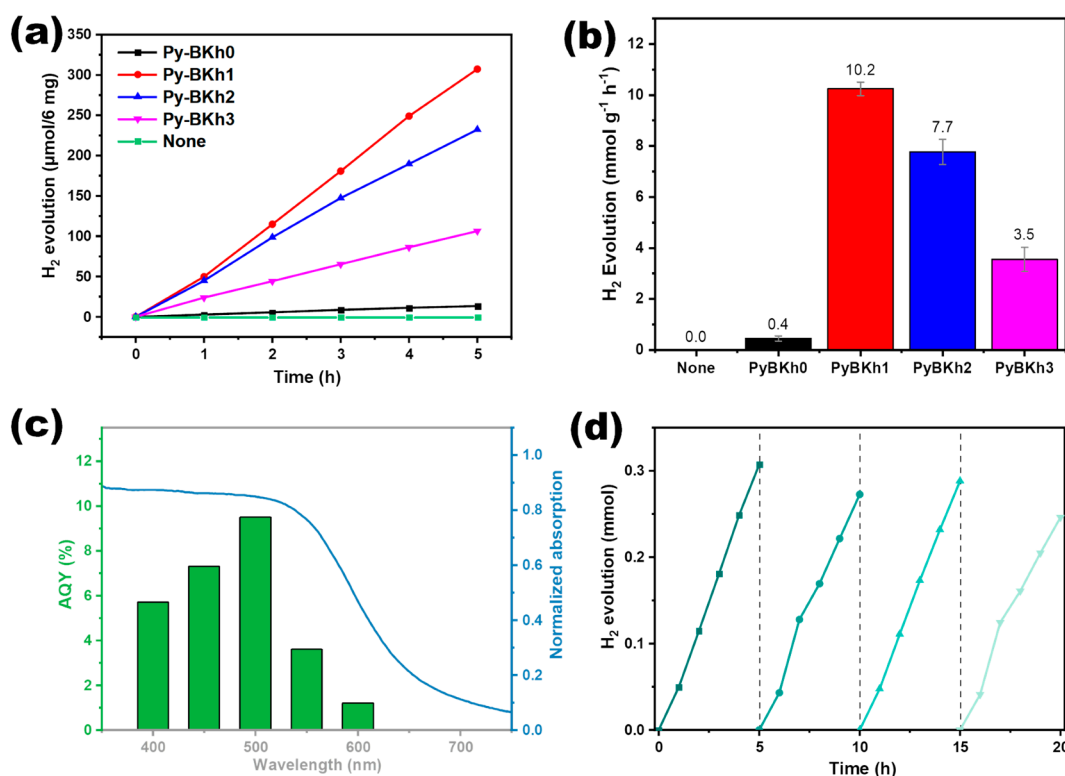

Figure 3. (**a**) Hydrogen production rate over time, (**b**) normalized HER for all CPPs, (**c**) AQY of Py-BKh1 at different wavelengths, (**d**) cyclic hydrogen production test for Py-BKh1.

To evaluate solar-to-hydrogen conversion efficiency, the apparent quantum yield (AQY) of Py-BKh1 was measured under monochromatic light (Figure 3c). Using a 6 mg catalyst with only water and ascorbic acid, AQYs reached 5.7%, 7.3%, 9.5%, 3.6%, and 1.2% at 400, 450, 500, 550, and 600 nm, respectively, consistent with its UV–vis absorption profile. The maximum AQY of 9.5% at 500 nm confirms efficient light utilization in the visible range and validates the photo-driven nature of hydrogen generation. Cycling tests assessed the stability of Py-BKh1 over 20 h (four cycles). As shown in Figure 3d, the HER gradually declined but retained ~80% of its initial activity, demonstrating robust stability. The slight activity recovery in the third cycle is attributed to the replenishment of the sacrificial agent (ascorbic acid), confirming that the catalyst retains structural integrity during prolonged operation. These results underscore the practical potential of the D_1-A-D_2 ternary design for sustainable photocatalytic hydrogen production. To check the residual Pd contents of the CPPs and its effect on HER, we altered the Pd catalyst to synthesize three batches of Py-BKh1 by using 2 mol%, 4 mol%, and 6 mol% Pd$_2$(dba)$_3$, which are accordingly denoted as Py-BKh1-2, Py-BKh1-4, and Py-BKh1-6, respectively. The ICP-MS test reveals that all CPPs exhibited almost equal residual Pt loading (~0.6 wt%, Table 1), which could be attributed to the saturation of Pd loaded on the CPPs after the identical post-treatment procedures. The hydrogen production tests on these three CPPs showed a slight increase in HER with an increase in Pd pre-catalyst loadings. This may be attributed to the increase in polymerization degrees due to the increased Pd loadings of the Pd catalyst. The effect of residual Pd and the polymerization degree on the photocatalytic performance explored here also coincides with previous studies [50].

Table 1. Remaining Pd and HER of Py-BKh1 synthesized by different amounts of Pd catalysts.

Material	$Pd_2(dba)_3$ [a] (mol%)	W (Pd) [b] (wt%)	H_2 Evolution Rate (mmol h^{-1} g^{-1})
Py-BKh1-2	2.0	0.6636	8.8
Py-BKh1-4	4.0	0.6154	10.2
Py-BKh1-6	6.0	0.6347	12.5

[a] SBED-BT$_{0.5\%}$ synthesized using $Pd_2(dba)_3$ with different feed ratios; [b] The Remaining Pd in the polymers obtained by Agilent ICP-MS 7700.

Meanwhile, the Py-BKh1 was recovered for structural analysis, and no observable changes occurred in the UV−vis and FT-IR spectra compared to the as-prepared one (Figure 4), manifesting the long-term stability of Py-BKh1 in the photocatalytic hydrogenation reaction. To enable comprehensive comparison, Table 2 summarizes the HER of Py-BKh1 and reference polymer photocatalysts. The results demonstrate that Py-BKh1 stands as one of the top-performing candidates among reported polymeric photocatalysts to date.
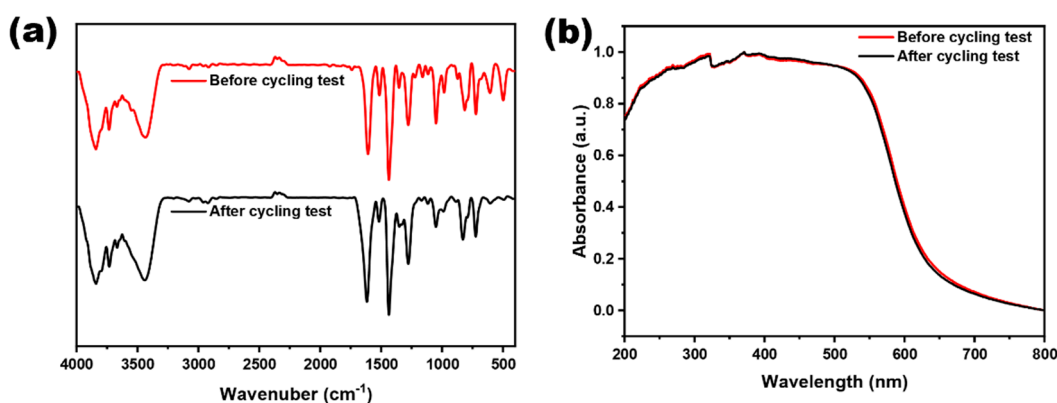
Figure 4. (**a**) UV−vis DRS and (**b**) FT-IR spectra of Py-BKh1 before and after recycling tests.

Table 2. Summary of photocatalytic hydrogenolysis reactions of photocatalysts.

Pub Date	Materials	H_2 Yield (mmol h^{-1} g^{-1})	AQY	Ref.
This Work	Py-BKh1	10.2	9.5% (500 nm)	-
2025.4	M-TiO$_2$-7	1.3	-	[51]
2025.3	ST@BTTA-120	3.69	-	[52]
2025.3	PFBT-Pdots	2.23	-	[53]
2025.2	SCN-0.5	1.67	5.8% (420 nm)	[54]
2024.9	PyBT-COF-COOH	8.15	5.1% (420 nm)	[55]
2024.7	Py-T-BTDO-3	8.66	4.42% (420 nm)	[56]
2024.6	PDTPDPA-BP	2.16	-	[57]
2023.11	NPs-TpPa-1	1.13	13.5% (450 nm)	[58]
2023.9	Zn-Por-TPT	11.45	-	[59]

3. Materials and Methods

3.1. Methods

All of the starting materials and reagents were purchased from commercial suppliers (Aladdin, Shanghai, China) and used directly without further purification. Anhydrous toluene was pretreated with calcium hydride (CaH_2) and freshly distilled.

FT-IR spectra were collected on a FT-IR spectrometer (Bruker ALPHA), and the KBr was mixed with the sample for sample preparation. Solid-state magic angle spinning [13]C

NMR measurements were carried out on a Bruker NEO WB 400M model 400 MHz NMR spectrometer at a MAS rate of 10 kHz. SEM images and TEM images of the polymers were obtained by scanning electron microscopy (SEM, MLA650F, Hillsboro, OR, USA) and transmission electron microscopy (TEM, FEI Tecnai G2 F20, USA). We recorded polymer photoluminescence (PL) conductivity by employing a HORIBA FL-1000 fluorescence spectrometer for solid powders. The photocatalytic output of hydrogen was quantitatively and qualitatively detected by gas chromatography (GC9790). The solid UV–visible absorption spectra of the synthesized polymers were detected by a UV-2600 spectrophotometer using $BaSO_4$ as a substrate reference. Transient photoresponse tests and electrochemical impedance spectroscopy were performed using a three-electrode configuration electrochemical workstation (CHI650E/700E, Shanghai Huachen Co., Ltd., Shanghai, China), where transient photocurrents and electrochemical impedances were measured using a platinum electrode as the auxiliary electrode and a silver/silver chloride electrode containing saturated potassium chloride solution as the reference electrode. The polymer was ultrasonically dispersed with ethanol to form a suspension, which was then dripped onto ITO conductive glass to form a sample with an effective area of 0.6 cm × 0.6 cm, and tested in a 0.1 M aqueous sodium sulfate solution as the electrolyte. Cyclic voltammetry testing is performed by using an electrochemical workstation (CHI650E/700E, Huachen Co LTD, Shanghai, China). The Pd metal residue was obtained by Agilent ICP-MS 7700, weighed a fixed measure of the sample, with an added 3 mL of HCl and 1 mL of HNO_3, microwave-heated at 180 °C for 30 min, and then transferred to a fixed volume for measurement. Elemental analyses of the polymers were obtained by Elimonta UNICUBE.

3.2. Synthesis of bis(2-thiophene)ketone, Py-BKh0, Py-BKh1, Py-BKh2, and Py-BKh3

Bis(2-thiophene)ketone: Firstly, the vacuum and argon substitution operation was repeated three times on the three-necked round-bottomed flask through the double-row tube, and, under the protection of argon atmosphere, $AlCl_3$ (36.6 mmol, 4.9 g) and anhydrous CH_2Cl_2 (1.5 mL) were added sequentially, the reaction temperature was controlled in the range of 0–4 °C, and the content of the flask was stirred for 10 min. Then, 2-thiophenecarbonyl chloride (9.1 mmol, 2.0 g) was dissolved in anhydrous CH_2Cl_2 and added into a dropping funnel, slowly dripped into the reaction flask and stirred for 10 min. Finally, thiophene (19 mmol, 1.6 g) was dissolved in anhydrous CH_2Cl_2 and added to the dropping funnel, slowly dripped into the reaction flask and stirred for 20 min, returned to room temperature, and reacted overnight. The product was poured into a mixture of 2 M HCl and ice water, the organic phase was collected by extraction and dried with anhydrous Na_2SO_4, the solvent was removed by rotary evaporation under vacuum, and the product was purified by column chromatography to give a light-yellow solid in 80% yield (1.4 g). ^{1}H NMR (400 MHz, Chloroform-d) δ 7.95 −7.87 (m, 2H), 7.74 −7.66 (m, 2H), and 7.22 −7.15 (m, 2H). ^{1}H NMR spectra are shown in the Supporting Information.

Procedure A: A proportion of 1,3,6,8-tetrabromopyrene (TBPy), bis(2-thiophene)ketone (BTK), 5,5′-dibromo-2,2′-bithiophene (DBBTh), anhydrous cesium carbonate (Cs_2CO_3), valerianic acid (PivOH), tris(dibenzylidene acetone)dipalladium ($Pd_2(dba)_3$), and (*o*-methoxyphenyl)phosphine (P(*o*-MeOPh)$_3$) were added into the Schlenk tube. The system was subjected to three cycles of vacuum and argon purging to ensure an oxygen-free environment. Anhydrous toluene was then added as the solvent under argon atmosphere, followed by three freeze–pump–thaw cycles to further remove residual oxygen. The reaction mixture was stirred continuously in an oil bath at 110 °C for 48 h. After the reaction, the crude product was cooled to room temperature and washed with dichloromethane, methanol, water and methanol, respectively, to remove small-molecule products and inorganic salts, and then dried under vacuum at 80 °C for 12 h to obtain the final product.

Py-BKh0: 1,3,6,8-tetrabromopyrene (1 eq, 133.3 mg), bis(2-thienyl)ketone (2 eq, 100.0 mg), Cs_2CO_3 (4 eq, 335.4 mg), PivOH (0.6 eq, 15.8 mg), catalyst $Pd_2(dba)_3$ (0.04 eq, 7.1 mg), and ligand $P(o\text{-MeOPh})_3$ (0.08 eq, 5.4 mg), reaction solvent anhydrous toluene of 6 mL. Following the description in Procedure A, the final product Py-BKh0 (137.0 mg, 90.7%) was obtained. IR (cm^{-1}): 1600, 1515, 1400, and 820. ^{13}C NMR (400 MHz, ppm) 177, 150, and 128.

Py-BKh1: 1,3,6,8-tetrabromopyrene (0.9 eq, 180.0 mg), bis(2-thienyl)ketone (2 eq, 100.0 mg), 5,5′-Dibromo-2,2′-bithiophene (0.2 eq, 25.0 mg), Cs_2CO_3 (4 eq, 335.4 mg), PivOH (0.6 eq, 15.8 mg), catalyst $Pd_2(dba)_3$ (0.04 eq, 7.1 mg), and ligand $P(o\text{-MeOPh})_3$ (0.08 eq, 5.4 mg), reaction solvent anhydrous toluene of 6 mL. Following the description in Procedure A, the final product Py-BKh1 (208.1 mg, 91.3%) was obtained. IR (cm^{-1}): 1600, 1515, 1400, and 820. ^{13}C NMR (400 MHz, ppm) 177, 150, 142, and 128.

Py-BKh2: 1,3,6,8-tetrabromopyrene (0.8 eq, 160.0 mg), bis(2-thienyl)ketone (2 eq, 100.0 mg), 5,5′-Dibromo-2,2′-bithiophene (0.4 eq, 50.0 mg), Cs_2CO_3 (4 eq, 335.4 mg), PivOH (0.6 eq, 15.8 mg), catalyst $Pd_2(dba)_3$ (0.04 eq, 7.1 mg), and ligand $P(o\text{-MeOPh})_3$ (0.08 eq, 5.4 mg), reaction solvent anhydrous toluene of 6 mL. Following the description in Procedure A, the final product Py-BKh2 (197.1 mg) was obtained. IR (cm^{-1}): 1600, 1515, 1400, and 820. ^{13}C NMR (400 MHz, ppm) 177, 150, 142, and 128.

Py-BKh3: 1,3,6,8-tetrabromopyrene (0.7 eq, 140.0 mg), bis(2-thienyl)ketone (2 eq, 100.0 mg), 5,5′-Dibromo-2,2′-bithiophene (0.6 eq, 75.0 mg), Cs_2CO_3 (4 eq, 335.4 mg), PivOH (0.6 eq, 15.8 mg), catalyst $Pd_2(dba)_3$ (0.04 eq, 7.1 mg), and ligand $P(o\text{-MeOPh})_3$ (0.08 eq, 5.4 mg), reaction solvent anhydrous toluene of 6 mL. Following the description in Procedure A, the final product Py-BKh3 (213.1 mg, 91.5%) was obtained. IR (cm^{-1}): 1600, 1515, 1400, and 820. ^{13}C NMR (400 MHz, ppm) 177, 150, 142, and 128.

4. Conclusions

Herein, we synthesized a donor (D)-acceptor (A) binary CPP via C–H/C–Br cross-coupling reactions using 1,3,6,8-tetrabromopyrene (TBPy) and bis(2-thienyl)ketone (BTK). Subsequently, a ternary D_1-A-D_2 CPP was constructed by incorporating 5,5′-dibromo-2,2′-bithiophene (DBBTh) as a secondary donor (D_2). Under visible-light irradiation ($\lambda > 420$ nm), the Py-BKh1(D_1:A:D_2 = 0.9:2:0.2) photocatalyst exhibited a hydrogen evolution rate (HER) of 10.2 mmol h^{-1} g^{-1} with an apparent quantum yield (AQY) of 9.5% at 500 nm. Systematic characterization revealed that the introduction of DBBTh significantly enhanced the CPPs' light-harvesting capability and proton (H^+) reduction capacity, enabling stronger charge carrier generation. This study employs copolymerization and diversified linkage strategies to modify polymeric structures, emphasizing the critical roles of visible-light absorption and charge transport in photocatalytic hydrogen production. Our findings provide a rational design framework for optimizing polymer architectures and electronic properties, paving the way for enhanced photocatalytic activity.

Author Contributions: Methodology and synthesis, Z.-H.X. and Y.-J.Z.; manuscript drafting, Z.-H.X. and J.L.; photocatalytic hydrogen production test, Y.-J.Z.; data analysis, Z.-H.X.; conceptualization, S.-Y.L.; writing—review and editing, J.L. and S.-Y.L.; supervision, S.-Y.L.; project administration, S.-Y.L.; funding acquisition, J.L. and S.-Y.L.; S.-Y.L. provided guidance during all stages. All authors have read and agreed to the published version of the manuscript.

Institutional Review Board Statement: Not applicable.

Informed Consent Statement: Not applicable.

Data Availability Statement: Data are contained within this article and Supplementary Materials.

Conflicts of Interest: The authors declare that they have no conflicts of interest.

References

1. Fujishima, A.; Honda, K. Electrochemical photolysis of water at a semiconductor electrode. *Nature* **1972**, *238*, 37–38. [CrossRef] [PubMed]
2. Meng, A.; Zhang, L.; Cheng, B.; Yu, J. Dual cocatalysts in TiO_2 photocatalysis. *Adv. Mater.* **2019**, *31*, 1807660. [CrossRef] [PubMed]
3. Wang, W.; Tadé, M.O.; Shao, Z. Nitrogen-doped simple and complex oxides for photocatalysis: A review. *Prog. Mater. Sci.* **2018**, *92*, 33–63. [CrossRef]
4. Cheng, L.; Xiang, Q.; Liao, Y.; Zhang, H. CdS-based photocatalysts. *Energy Environ. Sci.* **2018**, *11*, 1362–1391. [CrossRef]
5. Li, X.; Wu, X.; Liu, S.; Li, Y.; Fan, J.; Lv, K. Effects of fluorine on photocatalysis. *Chin. J. Catal.* **2020**, *41*, 1451–1467. [CrossRef]
6. Yanagida, S.; Kabumoto, A.; Mizumoto, K.; Pac, C.; Yoshino, K. Poly (p-phenylene)-catalysed photoreduction of water to hydrogen. *Chem. Commun.* **1985**, *8*, 474–475. [CrossRef]
7. Wang, X.; Maeda, K.; Thomas, A.; Takanabe, K.; Xin, G.; Carlsson, J.M.; Domen, K.; Antonietti, M. A metal-free polymeric photocatalyst for hydrogen production from water under visible light. *Nat. Mater.* **2009**, *8*, 76–80. [CrossRef]
8. Fan, X.; Zhang, L.; Cheng, R.; Wang, M.; Li, M.; Zhou, Y.; Shi, J. Construction of graphitic C_3N_4-based intramolecular donor–acceptor conjugated copolymers for photocatalytic hydrogen evolution. *ACS Catal.* **2015**, *5*, 5008–5015. [CrossRef]
9. Yang, C.; Cheng, B.; Xu, J.; Yu, J.; Cao, S. Donor-acceptor-based conjugated polymers for photocatalytic energy conversion. *EnergyChem.* **2024**, *6*, 100116. [CrossRef]
10. Qiao, S.; Di, M.; Jiang, J.-X.; Han, B.-H. Conjugated porous polymers for photocatalysis: The road from catalytic mechanism, molecular structure to advanced applications. *EnergyChem.* **2022**, *4*, 100094. [CrossRef]
11. Dai, C.; Liu, B. Conjugated polymers for visible-light-driven photocatalysis. *Energy Environ. Sci.* **2020**, *13*, 24–52. [CrossRef]
12. Zhang, G.; Lan, Z.A.; Wang, X. Conjugated polymers: Catalysts for photocatalytic hydrogen evolution. *Angew. Chem. Int. Ed.* **2016**, *55*, 15712–15727. [CrossRef] [PubMed]
13. Byun, J.; Zhang, K.A. Designing conjugated porous polymers for visible light-driven photocatalytic chemical transformations. *Mater. Horiz.* **2020**, *7*, 15–31. [CrossRef]
14. Yang, C.; Ma, B.C.; Zhang, L.; Lin, S.; Ghasimi, S.; Landfester, K.; Zhang, K.A.; Wang, X. Molecular engineering of conjugated polybenzothiadiazoles for enhanced hydrogen production by photosynthesis. *Angew. Chem. Int. Ed.* **2016**, *55*, 9202–9206. [CrossRef]
15. Zhao, Y.; Ma, W.; Xu, Y.; Zhang, C.; Wang, Q.; Yang, T.; Gao, X.; Wang, F.; Yan, C.; Jiang, J.-X. Effect of linking pattern of dibenzothiophene-S, S-dioxide-containing conjugated microporous polymers on the photocatalytic performance. *Macromolecules* **2018**, *51*, 9502–9508. [CrossRef]
16. Tan, Z.R.; Xing, Y.Q.; Cheng, J.Z.; Zhang, G.; Shen, Z.Q.; Zhang, Y.J.; Liao, G.; Chen, L.; Liu, S.Y. EDOT-based conjugated polymers accessed via C-H direct arylation for efficient photocatalytic hydrogen production. *Chem. Sci.* **2022**, *13*, 1725–1733. [CrossRef]
17. Hu, Z.; Wang, Z.; Zhang, X.; Tang, H.; Liu, X.; Huang, F.; Cao, Y. Conjugated polymers with oligoethylene glycol side chains for improved photocatalytic hydrogen evolution. *iScience* **2019**, *13*, 33–42. [CrossRef]
18. Woods, D.J.; Hillman, S.A.J.; Pearce, D.; Wilbraham, L.; Flagg, L.Q.; Duffy, W.; McCulloch, I.; Durrant, J.R.; Guilbert, A.A.Y.; Zwijnenburg, M.A.; et al. Side-chain tuning in conjugated polymer photocatalysts for improved hydrogen production from water. *Energy Environ. Sci.* **2020**, *13*, 1843–1855. [CrossRef]
19. Cho, S.; Seo, J.H.; Kim, S.H.; Song, S.; Jin, Y.; Lee, K.; Suh, H.; Heeger, A.J. Effect of substituted side chain on donor-acceptor conjugated copolymers. *Appl. Phys. Lett.* **2008**, *93*, 263301. [CrossRef]
20. Wang, L.; Zhu, W. Organic donor-acceptor systems for photocatalysis. *Adv. Sci.* **2024**, *11*, 2307227. [CrossRef]
21. Bhattacharjee, S.; Mondal, S.; Ghosh, A.; Banerjee, S.; Das, A.K.; Bhaumik, A. Rational design of highly porous donor–acceptor based conjugated microporous polymer for photocatalytic benzylamine coupling reaction. *Small* **2024**, *20*, 2406723. [CrossRef] [PubMed]

22. Yu, J.; Sun, X.; Xu, X.; Zhang, C.; He, X. Donor-acceptor type triazine-based conjugated porous polymer for visible-light-driven photocatalytic hydrogen evolution. *Appl. Catal. B Environ.* **2019**, *257*, 117935. [CrossRef]

23. Li, Z.; Fang, H.; Chen, Z.; Zou, W.; Zhao, C.; Yang, X. Regulating donor-acceptor interactions in triazine-based conjugated polymers for boosted photocatalytic hydrogen production. *Appl. Catal. B Environ.* **2022**, *312*, 121374. [CrossRef]

24. Yan, Y.; Yu, X.; Shao, C.; Hu, Y.; Huang, W.; Li, Y. Atomistic structural engineering of conjugated microporous polymers promotes photocatalytic biomass valorization. *Adv. Funct. Mater.* **2023**, *33*, 2304604. [CrossRef]

25. Yang, C.; Xiang, Y.; Wang, W.; Cheng, B.; Yang, K.; Yu, J.; Cao, S. Enhancing photocatalytic H_2O_2 production of donor$-$acceptor polymers by modulation of polymerization modes. *Appl. Catal. B Environ.* **2025**, *365*, 124856. [CrossRef]

26. Hu, Y.; Huang, W.; Wang, H.; He, Q.; Zhou, Y.; Yang, P.; Li, Y.; Li, Y. Metal-free photocatalytic hydrogenation using covalent triazine polymers. *Angew. Chem. Int. Ed.* **2020**, *59*, 14378–14382. [CrossRef]

27. Hayat, A.; Rahman, M.U.; Khan, I.; Khan, J.; Sohail, M.; Yasmeen, H.; Liu, S.Y.; Qi, K.; Lv, W. Conjugated electron donor-acceptor hybrid polymeric carbon nitride as a photocatalyst for CO_2 reduction. *Molecules* **2019**, *24*, 1779. [CrossRef]

28. Ye, D.; Liu, L.; Zhang, Y.; Qiu, J.; Tan, Z.; Xing, Y.; Liu, S. Tunable donor-acceptor linear conjugated polymers involving cyanostyrylthiophene linkages for visible-light-driven hydrogen production. *Molecules* **2023**, *28*, 2203. [CrossRef]

29. Liu, J.; Zhang, S.; Long, X.; Jin, X.; Zhu, Y.; Duan, S.; Zhao, J. Triazine and fused thiophene-based donor-acceptor type semiconducting conjugated polymer for enhanced visible-light-induced H_2 production. *Molecules* **2024**, *29*, 2807. [CrossRef]

30. Szuromi, P. Tuning band gaps with three halides. *Science* **2020**, *367*, 1086–1088.

31. Niu, W.; Ma, J.; Feng, X. Precise structural regulation and band-gap engineering of curved graphene nanoribbons. *Acc. Chem. Res.* **2022**, *55*, 3322–3333. [CrossRef] [PubMed]

32. Xie, Z.; Wang, W.; Ke, X.; Cai, X.; Chen, X.; Wang, S.; Lin, W.; Wang, X. A heptazine-based polymer photocatalyst with donor-acceptor configuration to promote exciton dissociation and charge separation. *Appl. Catal. B Environ.* **2023**, *325*, 122312. [CrossRef]

33. Xu, Y.; Mao, N.; Zhang, C.; Wang, X.; Zeng, J.; Chen, Y.; Wang, F.; Jiang, J.-X. Rational design of donor-π-acceptor conjugated microporous polymers for photocatalytic hydrogen production. *Appl. Catal. B Environ.* **2018**, *228*, 1–9. [CrossRef]

34. Shu, C.; Han, C.; Yang, X.; Zhang, C.; Chen, Y.; Ren, S.; Wang, F.; Huang, F.; Jiang, J.X. Boosting the photocatalytic hydrogen evolution activity for D–π–A conjugated microporous polymers by statistical copolymerization. *Adv. Mater.* **2021**, *33*, 2008498. [CrossRef]

35. Huang, W.-Y.; Shen, Z.-Q.; Cheng, J.-Z.; Liu, L.-L.; Yang, K.; Chen, X.; Wen, H.-R.; Liu, S.-Y. C–H activation derived CPPs for photocatalytic hydrogen production excellently accelerated by a DMF cosolvent. *J. Mater. Chem. A* **2019**, *7*, 24222–24230. [CrossRef]

36. Gong, H.; Li, J.; Xie, Z.-H.; Lang, C.; Liu, S.-Y. Accessing poly (DA-ran-Dπ) ternary copolymers via direct C–H arylation for ultrahigh photocatalytic hydrogen production. *Macromolecules* **2024**, *57*, 7208–7218. [CrossRef]

37. Lang, C.; Gong, H.; Ye, G.; Murugan, P.; Xie, Z.-H.; Dai, Y.-F.; Yang, K.; Yu, C.; Liu, S.-Y. D1-D2-Aternary conjugated microporous polymers synthesized via direct CH arylation for enhancing photocatalytic hydrogen evolution. *J. Colloid Interface Sci.* **2025**, *688*, 818–829. [CrossRef]

38. Wu, K.; Liu, X.-Y.; Xie, M.; Cheng, P.-W.; Zheng, J.; Lu, W.; Li, D. Rational design of D$-$π$-$A$-$π$-$D porous organic polymer with polarized π for photocatalytic aerobic oxidation. *Appl. Catal. B Environ.* **2023**, *334*, 122847. [CrossRef]

39. Yu, F.; Zhu, Z.; Wang, S.; Wang, J.; Xu, Z.; Song, F.; Dong, Z.; Zhang, Z. Novel donor-acceptor-acceptor ternary conjugated microporous polymers with boosting forward charge separation and suppressing backward charge recombination for photocatalytic reduction of uranium (VI). *Appl. Catal. B Environ.* **2022**, *301*, 120819. [CrossRef]

40. Wang, Z.; Qin, C.; Zhao, D.; Wang, Z.; Mao, D. Adsorption behavior of a ternary covalent organic polymer anchored with SO_3H for ciprofloxacin. *Molecules* **2023**, *28*, 6941. [CrossRef]

41. Sprick, R.S.; Jiang, J.X.; Bonillo, B.; Ren, S.; Ratvijitvech, T.; Guiglion, P.; Zwijnenburg, M.A.; Adams, D.J.; Cooper, A.I. Tunable organic photocatalysts for visible-light-driven hydrogen evolution. *J. Am. Chem. Soc.* **2015**, *137*, 3265–3270. [CrossRef] [PubMed]

42. Guo, L.; Niu, Y.; Razzaque, S.; Tan, B.; Jin, S. Design of D–A1–A2 covalent triazine frameworks via copolymerization for photocatalytic hydrogen evolution. *ACS Catal.* **2019**, *9*, 9438–9445. [CrossRef]

43. Wu, Y.; He, X.-Y.; Huang, X.-M.; Yang, L.-J.; Liu, P.; Chen, N.; Li, C.-Z.; Liu, S.-Y. Synthesis of Long Chain Oligomeric Donor and Acceptors via Direct Arylation for Organic Solar Cells. *Chin. J. Chem.* **2024**, *42*, 523–532. [CrossRef]

44. Liu, H.; Chen, Y.; Chen, N.; Liu, S.-Y. Stepwise Extended π$-$Conjugation Lengths of Chlorinated Oligomeric Non-fullerene Acceptors Accessed via Direct C$-$H Arylation. *Acta Polym. Sin.* **2023**, *54*, 1122–1130.

45. Xie, Z.H.; Ye, G.; Gong, H.; Pachaiyappan, M.; Lang, C.; Dai, Y.F.; Liu, S.Y. Ultrahigh photocatalytic hydrogen evolution of linear conjugated terpolymer enabled by an ultra-low ratio of benzothiadiazole monomer. *Chem. Sci.* **2025**. [CrossRef]

46. Li, L.; Zhang, Z.; Ding, C.; Xu, J. Boosting charge separation and photocatalytic CO_2 reduction of $CsPbBr_3$ perovskite quantum dots by hybridizing with P_3HT. *Chem. Eng. J.* **2021**, *419*, 129543. [CrossRef]

47. Biswal, B.P.; Vignolo-González, H.A.; Banerjee, T.; Grunenberg, L.; Savasci, G.; Gottschling, K.; Nuss, J.; Ochsenfeld, C.; Lotsch, B.V. Sustained solar H$_2$ evolution from a thiazolo, [.5.; 4-d] thiazole-bridged covalent organic framework nickel-thiolate cluster in water. *J. Am. Chem. Soc.* **2019**, *141*, 11082–11092. [CrossRef]

48. Xu, J.; Yang, C.; Bi, S.; Wang, W.; He, Y.; Wu, D.; Liang, Q.; Wang, X.; Zhang, F. Vinylene-linked covalent organic frameworks (COFs) with symmetry-tuned polarity and photocatalytic activity. *Angew. Chem.* **2020**, *132*, 24053–24061. [CrossRef]

49. Zhao, W.; Luo, L.; Cong, M.; Liu, X.; Zhang, Z.; Bahri, M.; Li, B.; Yang, J.; Yu, M.; Liu, L.; et al. Nanoscale covalent organic frameworks for enhanced photocatalytic hydrogen production. *Nat. Commun.* **2024**, *15*, 6482. [CrossRef]

50. Li, L.; Cai, Z.; Wu, Q.; Lo, W.Y.; Zhang, N.; Chen, L.X.; Yu, L. Rational design of porous conjugated polymers roles of residual palladium for photocatalytic hydrogen production. *J. Am. Chem. Soc.* **2016**, *138*, 7681–7686. [CrossRef]

51. Cervo, R.; Brandl, C.A.; Bortolotto, T.; Cechin, C.N.; Daudt, N.D.F.; Iglesias, B.A.; Lang, E.S.; Tirloni, B.; Cargnelutti, R. Structural Analysis of Selenium Coordination Compounds and Mesoporous TiO$_2$-Based Photocatalysts for Hydrogen Generation. *Inorg. Chem.* **2025**, *64*, 7902–7919. [CrossRef] [PubMed]

52. Huang, Z.; Wu, Y.; Yu, C.; Wang, Z.; Jin, C.; Li, Z.; Yin, S. Impact of the Donor–Acceptor Structure on Photocatalytic Hydrogen Generation by Polyfluorene Polymer Dots. *ACS Appl. Polym. Mater.* **2025**, *7*, 3399–3408. [CrossRef]

53. Gao, T.; Liu, X.; Wang, K.; Wang, J.; Wu, X.; Wang, G. Sponge-like inorganic–organic S-scheme heterojunction for efficient photocatalytic hydrogen evolution. *J. Colloid Interface Sci.* **2025**, *692*, 137475. [CrossRef] [PubMed]

54. Wu, M.; Chen, L.; Sheng, Y.; Song, L.; Zhou, H.; Jian, J.; Huang, T.; Liu, B.; Li, X. Defects enriched carbon nitride sponge with high surface area for enhanced photocatalytic hydrogen evolution. *J. Colloid Interface Sci.* **2025**, *688*, 59–66. [CrossRef]

55. Yang, S.; Liu, W.; Zhang, Y.; Jia, X.; Sun, J.; Zhang, C.; Liu, M. Apost-modified donor–acceptor covalent organic framework for enhanced photocatalytic H2 production high proton transport. *J. Mater. Chem. A* **2024**, *12*, 28161–28169. [CrossRef]

56. Zhan, J.; Zhang, X.; Zhang, C.; Yang, Y.; Ding, X.; Ding, D.; Chai, B.; Dai, K.; Chen, H. Thienyl-fused dibenzothiophene-S, S-dioxide based conjugated polymer toward highly efficient photocatalytic hydrogen production. *Int. J. Hydrog. Energy* **2024**, *80*, 115–124. [CrossRef]

57. Wang, Y.; Wang, C.E.; Wang, W.R.; Li, Q.; Liu, L.N.; Xu, Z.W.; Gao, T.; Wang, Y.; Li, W.S. Conjugated diacetylene polymers with intrachain DA block heterostructure for efficient photocatalytic hydrogen production. *Polymer* **2024**, *308*, 127334. [CrossRef]

58. Zhao, Z.; Chen, W.; Zhang, G.; Chen, Y. Interface molecular wires induce electron transfer from COFs to Pt for enhanced photocatalytic H$_2$ evolution. *J. Mater. Chem. A* **2023**, *11*, 26052–26062. [CrossRef]

59. Zhang, G.; Elewa, A.M.; Rashad, M.; Helali, S.; Chou, H.H.; EL-Mahdy, A.F. Triazine-and porphyrin-based donor-acceptor microporous conjugated polymers for enhanced photocatalytic hydrogen production activity. *Microporous Mesoporous Mater.* **2023**, *363*, 112824. [CrossRef]